Mon. Not. R. Astron. Soc. **349,** 1449–1463 (2004) doi:10.1111/j.1365-2966.2004.07620.x

On the determination of age and mass functions of stars in young open star clusters from the analysis of their luminosity functions

A. E. Piskunov,[1⋆] A. N. Belikov,[1⋆] N. V. Kharchenko,[2⋆] R. Sagar[3,4⋆] and A. Subramaniam[4⋆]

[1]*Institute of Astronomy of the Russian Academy of Sciences, 48 Pyatnitskaya Str., Moscow 119017, Russia*
[2]*Main Astronomical Observatory, 27 Akademika Zabolotnogo Str., 03680 Kiev, Ukraine*
[3]*State Observatory, Manora Peak, Naini Tal 263129, India*
[4]*Indian Institute of Astrophysics, Bangalore 560034, India*

Accepted 2004 January 12. Received 2004 January 12; in original form 2003 June 27

ABSTRACT

We construct the observed luminosity functions of the remote young open clusters NGC 2383, 2384, 4103, 4755, 7510 and Hogg 15 from CCD observations of them. The observed LFs are corrected for field star contamination determined with the help of a Galactic star count model. In the case of Hogg 15 and NGC 2383 we also consider the additional contamination from neighbouring clusters NGC 4609 and 2384, respectively. These corrections provide a realistic pattern of cluster LF in the vicinity of the main-sequence (MS) turn-on point and at fainter magnitudes reveal the so-called H-feature arising as a result of the transition of the pre-MS phase to the MS, which is dependent on the cluster age. The theoretical LFs are constructed representing a cluster population model with continuous star formation for a short time-scale and a power-law initial mass function (IMF), and these are fitted to the observed LF. As a result, we are able to determine for each cluster a set of parameters describing the cluster population (the age, duration of star formation, IMF slope and percentage of field star contamination). It is found that in spite of the non-monotonic behaviour of observed LFs, cluster IMFs can be described as power-law functions with slopes similar to Salpeter's value. The present main-sequence turn-on cluster ages are several times lower than those derived from the fitting of theoretical isochrones to the turn-off region of the upper main sequences.

Key words: stars: luminosity function, mass function – open clusters and associations: general.

1 INTRODUCTION

Young clusters are natural laboratories for the study of various issues related to star formation processes, e.g. the initial mass function (IMF), duration of star formation etc. In recent years, some remote young clusters have been studied using *BVRI* CCD observations (e.g. see Sagar & Griffiths 1991; Phelps & Janes 1993; Sagar & Cannon 1995, 1997; Sagar & Griffiths 1998; Subramaniam & Sagar 1999; Sagar, Munari & de Boer 2001; Sanner et al. 2001; Pandey et al. 2001; Piatti et al. 2002). These observations were used for the construction of colour–colour diagrams, colour–magnitude diagrams (CMDs) and luminosity functions (LFs). These diagrams were used for the determination of cluster reddening, distance and age while the LFs were transformed to stellar mass spectrum, which can be identified with the IMF for young (age $\leqslant$100 Myr) star clusters. In these conventional studies of young star clusters, cluster age, LFs and MFs could not be determined accurately for reasons discussed below.

First, for reliable separation of cluster members from the foreground and background field stars present in the direction of distant ($d > 1$ kpc) clusters, accurate kinematic (proper motion and/or radial velocity) measurements are essential. Unfortunately, even present day, highly accurate *Hipparcos* proper motion data (available for the brightest $V < 13$ mag stars only) are not sufficient for this purpose. In such circumstances, the field star contamination is removed statistically by observing comparison areas (blank fields) adjacent to the cluster field. It should be noted, however, that in most cases of conventional general-purpose CCD photometry, which are not specially intended for e.g. the IMF study, such regions are not observed and, hence, even statistical means of data refining could not be used. This leads to a loss of information that is otherwise suitable for LF construction.

⋆E-mail: piskunov@inasan.rssi.ru (AEP); abelikov@ari.uni-heidelberg.de (ANB); nkhar@mao.kiev.ua (NVK); sagar@upso.ernet.in (RS); purni@iiap.res.in (AS)

The other problem in the CMDs of young star clusters is the precise determination of the main-sequence (MS) turn-off point, which is used for age determination, because for young clusters, as a result of their small age, the upper MS is practically unevolved. Consequently, it becomes difficult to evaluate the accurate cluster age and, instead, an upper estimate of the cluster age is provided. The difficulty is further increased by effects like stellar rotation and binarity, and by the morphology of the upper MS, which is practically vertical for early-type stars in the colours $(B-V)$, $(V-R)$ or $(V-I)$.

These problems can be avoided if the cluster age is estimated using the location of the MS turn-on point, the place where pre-MS stars join the MS in the cluster CMD. For a young coeval cluster this point resides at approximately 7 mag fainter than the brightest termination point of the MS. As a result of deep CCD observations of the clusters, this region can be seen in the CMD and, hence, is available for the analysis. Many of the above effects (except that of unresolved binaries) are much weaker in the turn-on point region, which makes the turn-on dating method more attractive than that of the turn-off. There are, however, practical problems in locating the turn-on point, for example, the presence of strong field star contamination hides it more strongly than the brightest MS. The other limitation of the turn-on method is cluster age. As shown by evolutionary calculations, only for extremely young clusters with ages of the order of a few Myr is the pre-MS branch raised sufficiently above the zero-age main-sequence(ZAMS) and can be easily recognized in the CMD. For older clusters the pre-MS branch deviation from the ZAMS diminishes with increasing age and can be seen better as a detail of the LF (as discussed in Section 2). At cluster ages exceeding that of the Pleiades, the pre-MS branch cannot be identified with confidence, either in the CMD or in the LF, and the turn-on method cannot be applied (Belikov et al. 1998).

The other related issue is the fine structure of the stellar LF, located in the vicinity of the MS turn-on point, which can mask the IMF shape if one does not take it into account. This feature can produce a false flattening or even depletion in the LF, which is frequently considered as evidence of the flattening/turning over of the IMF (see Piskunov & Belikov 1996, for references). This, in turn, might have an important consequence with respect to the IMF universality and other similar issues. Because the LF of the turn-on point depends on cluster age, the position of the LF detail also varies with time and may be used as a kind of standard candle for age determination from LF analysis (Belikov & Piskunov 1997).

Thus, the MS turn-on region of young cluster CMDs is very important for cluster dating, or should be taken into account when one is analysing the LF. It can only be easily identified, however, in the case of a few selected clusters. The well-known examples of such clusters are NGC 2264, NGC 6530, the Orion Nebula Cluster and some others. Normally, young and especially remote clusters, which are buried in a rich foreground/background, show neither distinct turn-on points nor PMS branches.

The aim of the present study is to reveal the MS turn-on point information hidden in the existing CCD observational data of six young open clusters using a new approach, which does not require observations of blank fields. It should be noted that these clusters were the subject of a conventional study, and many of them already have age and IMF determination. Unlike these studies, we will not convert the observed LF to the IMF, but in order to avoid the above mentioned problems we will construct a theoretical LF, which should properly reflect the behaviour of the observed LF in the vicinity of the MS turn-on point. Wherever the field star contaminations cannot be determined using the observations of an offset field region, they are estimated using a Galactic model for star counts for the surroundings of the cluster under study. Then, the theoretical LF will be fitted to the observations by varying the star formation parameters describing actual stellar population (cluster age, star formation duration, IMF slope, a percentage of observed field stars). Considering its success, we hope that this approach can also be implemented in the study of other young open clusters with similar or deeper CCD data, which are presently becoming available (see e.g. Kalirai et al. 2001).

In Section 2, we detail the theoretical approach to the LF of a young cluster and consider its fine structure in the context of the current study. In Section 3, we summarize the data used in the present work. Section 4 describes the construction of the observed and theoretical LFs: we consider the major effects that should be taken into consideration, define the model of the cluster population and its parameters, and describe the fitting procedure. In Section 5 we discuss the derived results and summarize them in Section 6.

2 THEORETICAL APPROACH

Because stellar mass m can be directly measured in very rare and specific cases, the IMF is not observed directly, but it is converted from the observed distribution of stars over their absolute magnitudes $\mathrm{d}N/\mathrm{d}M$, called the LF $\phi(M)$. For a cluster of age t (given in years throughout the paper, unless mentioned otherwise), the LF $\phi_t(M)$ is related to the IMF $f(m)$ via the time-dependent mass–luminosity relation (MLR) $m_t(M)$ as

$$\phi_t(M) = \frac{\mathrm{d}N}{\mathrm{d}\log m} \times \left|\frac{\mathrm{d}\log m}{\mathrm{d}M}\right|_t = f(m_t[M]) \times \left|\frac{\mathrm{d}\log m}{\mathrm{d}M}\right|_t . \quad (1)$$

Because cluster stars evolve off or approach the MS with a rate that is dependent on their mass, apart from their stay on the MS, the cluster MLR should also evolve with time, being different at every moment from the standard one (usually adopted to be the MLR of the MS stars). This deviation is especially strong for red giant and pre-MS stars. Besides, the instant MLR has a definite fine structure as a result of the presence of quasi-horizontal post- and pre-MS portions of the corresponding isochrone. The structure itself is not sufficiently prominent to influence the LF, but it produces bumps and dips in the MLR derivative and, hence, in the LF. The strongest fluctuation of the derivative occurs near the MS turn-off point, but as a result of the small number of stars observed there, it could not be easily distinguished from statistical fluctuations of the LF. In contrast, in the vicinity of the MS turn-on point, a sufficient number of stars coupled with strong MLR-derivative bumping produce a feature, which can be observed in LFs of star clusters that are young enough to display a branch of pre-MS stars. This detail was called an H-feature by Piskunov & Belikov (1996) as it appears at the location where hydrogen burning starts in the cores of the pre-MS stars.

In order to get an idea of the general structure of the LFs of young star clusters and their relation to the main evolutionary stages of stars, in Fig. 1 we show the CMD together with an isochrone of $\log t = 7.0$ and corresponding LF constructed according to equation (1) with the help of the Salpeter IMF $[f(m) \propto m^{-1.35}]$. The isochrone was constructed from a set of stellar models described in Section 4.4. Our calculations show that in general this behaviour of the LF does not differ for various sets of models, but the details (size and amplitude of LF fragments) may be somewhat different.

As one can see from Fig. 1, for young clusters the LF is non-monotonic even for a monotonic IMF and consists of a number of monotonic portions related to different evolutionary stages. Comparison with evolutionary tracks shows that segment (0, 1) of the

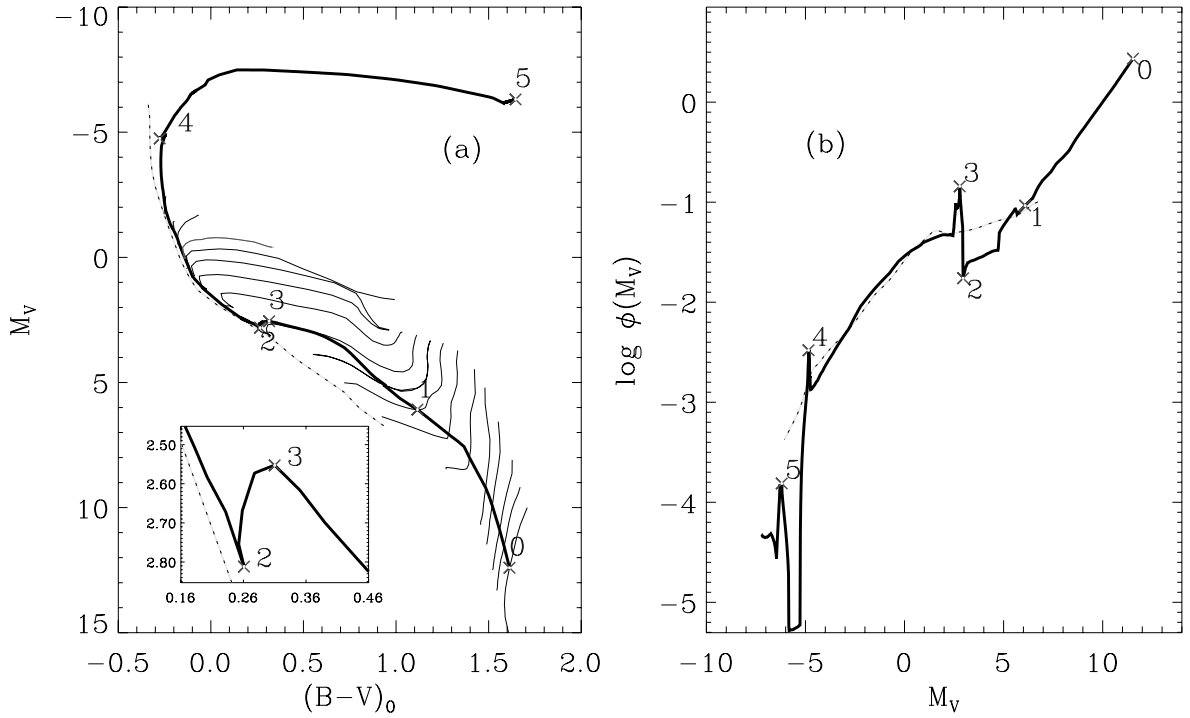

Figure 1. Theoretical colour–magnitude diagram (panel a) and luminosity function (panel b) of a young open cluster. The solid curves are for an isochrone of $\log t = 7.0$, including both pre- and post-MS evolutionary stages, and corresponding LF, constructed from the isochrone. The dotted curves are the ZAMS and main-sequence luminosity function. Thin curves in panel (a) are pre-MS evolutionary tracks of Palla & Stahler (1993). The crosses and adjacent figures separate different evolutionary stages as explained in the text. The enlarged MS turn-on point area is shown in the panel encapsulated in the CMD.

LF corresponds to the convective portion of a pre-MS track; (1, 2) corresponds to to the radiative one; (2, 3) can be identified with the MS turn-on point in the CMD; and segment (3, 4) belongs to the MS. As a result of the non-monotonic behaviour of the isochrone near the MS turn-on point, the segment (2, 3) is, in fact, a superposition of MS and pre-MS stellar evolutionary stages, and pure MS starts at somewhat brighter magnitudes. The last segment (4, 5) corresponds to post-MS stages of stellar evolution. Hereafter, for convenience, we call segment (1, 2) the LF H-dip and (2, 3) the LF H-maximum. For comparison in Fig. 1, we show the position of the ZAMS models of Tout et al. (1996) and the ZAMS-LF constructed from them. Good agreement between the ZAMS and LFs is observed between both turn-over points, but beyond the MS both LFs differ considerably.

Because the absolute magnitude of a cluster MS turn-on point evolves with time, the H-feature should move faint-ward with increasing cluster age. The feature not only moves to fainter magnitudes, but also degrades with time. As the calculations of Belikov & Piskunov (1997) show it disappears completely for $\log t \geqslant 8.2$; this puts a limit on the H-calibration applicability. Again the time-scale of existence of the H-feature depends on specific models and can be used for pre-MS model verification. In principle, this makes the LF of young clusters a good tool for cluster age determination.

An immediate conclusion, which could be drawn from the above analysis, is that the existence of any bumps/gaps in the LF at or near the MS turn-on point of young clusters should not be regarded as evidence of non-monotonic behaviour of the IMF. The existence of the pre-MS detail in the LF may also result in the misinterpretation of mass spectra of young open clusters. When the limiting magnitude of a survey falls within the radiative dip, one can observe the LF turnover, which can be wrongly interpreted as a consequence of data incompleteness or the IMF turnover. Similarly, the steep slope of the convective portion of the LF is not evidence of IMF steepening.

3 OBSERVATIONAL DATA

We have used CCD photometric data of young (age $\leqslant$ several tens of Myr) remote and compact clusters presented in the papers listed in Table 1 (hereafter referred to as 'original papers'). The small areas occupied by these clusters and their sufficiently deep photometry provide a high degree of data completeness, which is very important for LF construction. However, their large distance coupled with lack of kinematic data prevents the separation of cluster members from the field stars and requires a special approach to tackle this issue.

In Table 1 the parameters of the clusters under study are listed. Cluster designations are shown in columns 1 and 2; in column 3 we list values of cluster angular diameters taken from Lyngå (1987). Most of the other parameters are taken from the original papers previously mentioned. Columns 4 to 9 contain the area covered by CCD frames, number of stars within the frames, limiting and completeness V-magnitudes, apparent distance moduli and reddening values. Colour excesses, marked with asterisks, represent average values in variable extinction fields. In column 10 we show log (age) as it was determined in the studies referred to earlier. We define the limiting magnitude of a survey as the faintest magnitude of a star in a cluster sample. Data completenesses in magnitude are estimated following the procedure described in Section 4.3.

We compared the original data of Table 1 with the Lyngå (1987) catalogue and recent lists of reddening values, distance moduli and ages, provided by Loktin, Gerasimenko & Malysheva (2001) (referred to hereafter as LGM2.2). We find that the extinction values

Table 1. Specification of clusters studied and observational data used.

Cluster	IAU number	d'	Area (arcmin^2)	Number of stars	$V_{\rm lim}$ (mag)	$V_{\rm cmp}$ (mag)	$V-M_V$ (mag)	$E(B-V)$ (mag)	$\log t$	Reference
NGC 2383	C0722–208	5	31.8	588	21.8	17.6	13.3	0.22	8.45–8.6	(1)
NGC 2384	C0722–209	5	27.8	256	20.9	18.9	13.2	0.22–0.28	7.1–7.3	(1)
NGC 4103	C1204–609	5	19.4	176	19.8	17.3	12.5	0.31	7.5	(2)
Hogg 15	C1240–628	2	6.9	337	21.7	19.6	16.5	1.15*	6.78	(3)
NGC 4755	C1250–600	10	38.8	576	20.2	18.1	12.9	0.41*	7.0	(4)
NGC 7510	C2309+603	6	38.4	423	21.1	16.8	16.0	1.12*	<7.0	(5)

[1]Subramaniam & Sagar (1999), [2]Sagar & Cannon (1997), [3]Sagar, Munari & de Boer (2001), [4]Sagar & Cannon (1995), [5]Sagar & Griffiths (1991).
*Non-uniform extinction.

from Table 1 are in excellent agreement with the data of both catalogues and the average colour excesses from different lists agree within a few hundredths of a magnitude, except in the case of NGC 7510. In this case, the extinction data in LGM2.2 differ from that of Table 1 by 0.26 mag. Original cluster ages, also, show reasonable agreement (with an average spread of the order of a few tenths in $\log t$) for all clusters except NGC 2383, which according to both Lyngå (1987) and LGM2.2 has an age of a few tens of Myr.

Unfortunately, such a good agreement is not observed in the case of cluster distances. Comparison with the Lyngå (1987) distance estimations shows good agreement for all clusters, except NGC 2383 and 2384, where the data of Table 1 are overestimated by approximately 1 mag. The new scale of LGM2.2 indicates even stronger (up to 1.5 mag) disagreement for these and two more (Hogg 15 and NGC 7510) clusters. Though these disagreements are unpleasant, it is hardly avoidable as photometric distances of remote clusters are derived from a very steep upper MS. In the present study we will use original distances, keeping the above problems in mind.

The possible uncertainty in cluster age and the MF slope, which can be introduced by the data inaccuracy, can be estimated from the following considerations. The most important for our LF-based analysis is accuracy in absolute magnitude M_V. It depends on error in the distance modulus, reddening correction and a correction for metallicity effects. Because no metallicity measurements are published for the clusters under study, we can estimate this correction only indirectly. As the cluster galactocentric distances span a range of 7–11 kpc (with the solar value assumed to be 8.5 kpc), the metallicity radial gradient in the Galactic disc is absent according to the data on Cepheids of Andrievsky et al. (2002). Thus, we can accept the solar heavy-element abundance and avoid metallicity corrections. The spread of cluster metallicity can only be be the result of Galactic disc inhomogeneity, which according to Vereschagin & Piskunov (1992) is about Δ[Fe/H] ≈ 0.1. The corresponding absolute magnitude uncertainty resulting from the metallicity effect is of the order of $\Delta M_V \approx 0.1$ mag. The standard accuracy of the cluster apparent distance modulus is approximately 0.2 mag (Subramaniam & Sagar 1999). The reddening uncertainty according to original papers is between 0.03 and 0.06 mag and only for NGC 7510 does it exceed [$\sigma_{E(B-V)} = 0.09$ mag] the upper limit. These cause the M_V uncertainty to be typically approximately 0.1–0.2 mag and less than 0.3 mag for the complete sample. Thus, we believe that the aggregated uncertainty in absolute magnitude resulting from metallicity, interstellar extinction and distance modulus errors does not exceed 0.5 mag. This corresponds to a random error in $\log t$ of the order of 0.15 for both turn-off and turn-on dating methods. According to the simulations of Belikov (1999) one can expect an error in the MF slope caused by $\sigma_{M_V} = 0.5$ mag of the order of 0.2.

The original CCD photometry was complemented with photoelectric magnitudes of brighter stars from the sources referred to in the original papers and/or from the WEBDA data base. This extends the range of data completeness from a faint cluster-specific limit, discussed in Section 4.3, to the brightest in the observed field stars. Because the data in the V magnitude are the most complete we use in this study, LFs are constructed in V only.

As one can see from Table 1, stellar fields covered by the frames are comparable to the cluster sizes provided in the Lyngå (1987) catalogue. It should be noted, however, that Lyngå (1987) provides only sizes of the central parts of open clusters, which according to Kharchenko, Pakulyak & Piskunov (2003) are two to three times smaller than their full size. Similar conclusions have also been drawn by Nilakshi et al. (2002) based on a spatial structure study of open star clusters. Thus, we should consider our samples only as the inner population of the clusters, enhanced with massive stars (Kharchenko et al. 2003), and having flatter luminosity functions and mass spectra than the outer population (de Grijs et al. 2002a,b,c).

In Fig. 2 we show the wide neighbourhoods of the clusters under study. They are constructed with the help of all-sky catalogues ASCC-2.5[1] (Kharchenko 2001) for the brightest ($V < 13$ mag) stars and UCAC1[2] (Zacharias et al. 2000) [FONAC[3] (Kislyuk et al. 1999) in the NGC 7510 case] for fainter stars. In order to give the reader an idea of the relation of observed frames to cluster geometry, in the maps we show positions of cluster centres and borders of cluster cores and coronae, as determined by Kharchenko et al. (2003) from data on the spatial distribution of cluster proper motion members from the ASCC-2.5. For NGC 2383 Kharchenko et al. (2003) failed to detect the core radius and the core is not shown in the cluster map. Because the brightest stars of Hogg 15 are fainter than the limiting magnitude of the ASCC-2.5, the data on the cluster centre and radius were taken from Dias, Lépine & Alessi (2002) and Moffat (1974), respectively.

One can see from Fig. 2 that regions of two clusters (NGC 2383 and Hogg 15) are overlapped with their neighbouring clusters. This should be regarded as a potential source of cluster sample contamination and should be kept in mind in further discussions. NGC 4755 is the only cluster where observations are carried out in two separated frames located on both sides of the cluster centre.

[1] available at ftp://cdsarc.u-strasbg.fr/pub/cats/I/280A
[2] available at ftp://cdsarc.u-strasbg.fr/pub/cats/I/268
[3] available at ftp://cdsarc.u-strasbg.fr/pub/cats/I/261

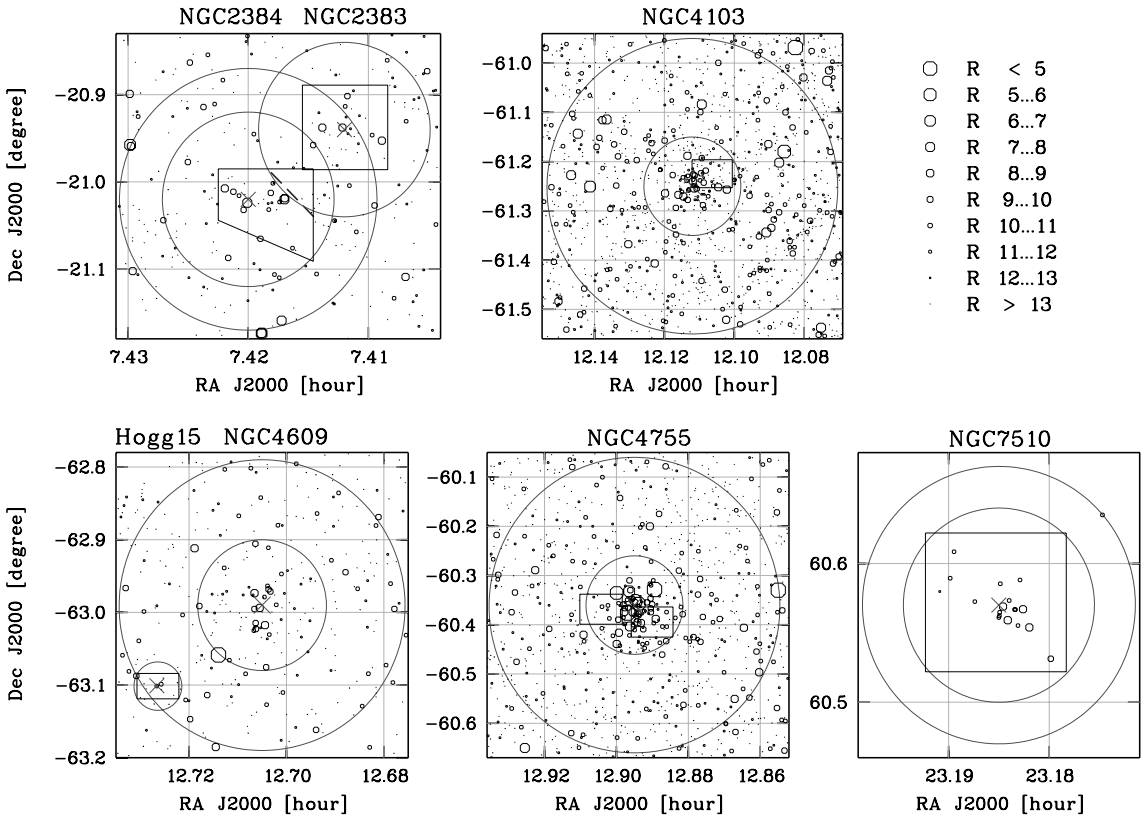

Figure 2. Maps of stellar fields in the vicinity of the studied clusters are constructed with the help of the ASCC-2.5, UCAC1 and FONAC catalogues. The size of the stellar images corresponds to stellar magnitude ($R_{\rm FONAC}$ for the case of NGC 7510 and R_u for the others): the magnitude scale is shown in the upper right corner. Crosses mark cluster centres. Large circles denote core and corona areas; solid quadrangles show CCD frames used.

4 OBSERVED AND THEORETICAL LUMINOSITY FUNCTIONS

Before comparing the empirical and theoretical LFs, it is necessary to correct the observed LF for different biases mentioned earlier. Among the most serious effects influencing the observed LFs are contamination of a cluster sample with non-members and data incompleteness. Generally, the non-members are field stars projected on to the cluster area, but in some cases, there will be stars from a neighbouring cluster also. The data incompleteness has a strong dependence on the crowding/density of stars in the field and the stellar magnitude, such that the data are less complete in crowded regions and towards fainter magnitudes (see e.g. Sagar & Richtler 1991). All these, as well as details of the procedure for the construction of the theoretical LF and fitting of theoretical and empirical LFs, will be described below.

4.1 Field star decontamination with a Galactic star count model

Depending on cluster distance and the properties of the observed sample, one can apply different methods for the selection of cluster members. For nearby clusters, the kinematic method is the most common and reliable. For remote clusters, statistical selection with the help of adjacent stellar fields is used. Because there are no blank fields observed in the neighbourhood of most of the clusters under study, we use Galactic star count models to estimate the field star contamination in their directions. As a result of various perturbations (e.g. resulting from spiral arms) along the line of sight, which can hardly be taken into account in detail by the model, this approach appears to be crude at first glance, especially for a study of the fine structure of the LF. A careful analysis indicates the contrary, however. It is well known that the leading role among a number of effects influencing the predicted apparent stellar density is played by interstellar extinction, as it is uneven over the Galactic disc. For example, the patchy behaviour of the extinction is the major factor enabling observation of remote clusters in transparency windows. This is a basic point of our approach because the extinction in a cluster direction can be derived with much more confidence when compared with an average extinction value in the disc; more realistic model predictions can be made in a cluster field than in an arbitrary stellar field. Below, we describe the model components, discuss the degree of model stability against extinction and stellar density fluctuations, and compare the model predictions with data on selected test fields.

For each cluster, we compute a theoretical distribution of field stars with apparent magnitude $\psi(V)$, which is specific to the cluster parameters, including Galactic coordinates and interstellar extinction towards the cluster, normalized to the area of the observed cluster region. We use the model described by Kharchenko & Schilbach (1996) and Kharchenko et al. (1997). The model treats the Galaxy as a system, which is symmetric with respect to both rotation axis and equatorial plane, and consists of three populations (thin disc, the disc hereafter, thick disc and a spheroid). The population of the thin disc consists of several subpopulations (MS stars, disc red giants and supergiants – stars of luminosity classes I and II). Each population group is described by its own stellar LF and spatial distribution. It is accepted that the population LF does not depend on position

within the Galaxy and is equal to its solar neighbourhood counterpart. Density distributions of different populations are represented by the expressions of Bahcall (1986) for disc-like and spheroidal subsystems.

The LF for MS stars brighter than $M_V = 13$ mag is taken from Scalo (1986) and Murray et al. (1997), while for fainter stars ($M_V \leqslant 19$ mag) we use data given by Jahreiß & Wielen (1997) for nearby stars. The fraction of evolved stars which have left the MS phase (red and supergiants) as a function of M_V was taken from Scalo (1986). These values are modified at $M_V \approx 0.75$ mag, $(B-V) \approx 1.0$ mag according to the data of Holmberg, Flinn & Lindengren (1997) taking into account the red giant clump, an equivalent of the Population II horizontal branch for disc-population core helium burning stars. The LFs of the thick disc and spheroid and the star number density normalization (thin disc : thick disc : spheroid) are 1 : 0.02 : 0.00125, taken from Gilmore (1984). Additionally, results by Da Costa (1982) for globular clusters are used to model the influence of the horizontal branch on the spheroid LF.

We adopt the following general parameters of the model: the galactocentric distance of the Sun is equal to 8.5 kpc; the ratio of axes of the spatial density distribution for the spheroid is equal to 0.85; the length-scale of the disc subsystems and the height-scale of the thick disc are equal to 4 and 1.3 kpc, respectively. We assume, according to Schmidt (1963) and Scalo (1986), that the height-scale of the disc for MS stars rises from 90 to 350 pc at M_V interval (2.3, 5.4) mag, whereas for red giants it changes from 250 to 400 pc at $M_V = (-0.75, 2.6)$ mag. The height-scale of 90 pc is used for extremely young populations of supergiants.

Young open clusters are located in the Galactic disc with irregular interstellar absorption and their extinction parameters differ from average Galactic values. This is a major reason for using cluster-specific absorption values a_V in model calculations, which are derived from the Parenago (1940) formula

$$A_V = \frac{a_V h_Z}{|\sin b|}\left[1 - \exp\left(\frac{-d|\sin b|}{h_Z}\right)\right], \qquad (2)$$

where d is the cluster distance from the Sun, b is the cluster Galactic latitude, $A_V = 3.1\,E(B-V)$ with $E(B-V)$ taken from Table 1 and h_Z is the height-scale of the extinction layer assumed to be equal to 100 pc.[4] Values of a_V together with cluster Galactic coordinates are shown in Table 2.

In order to illustrate the decisive role of the reddening effect in the model count construction, we have compared our results with calculations with a standard value of Galactic specific extinction $a_V^{\rm G} = 1.6$ mag kpc^{-1}, adopted for the Galactic disc. As shown by the comparison, for all clusters in the working magnitude range of $V = 10$–20 mag, the overestimation of specific extinction leads to considerable underestimation of the model density. The corresponding model curves differ in working magnitude range for different clusters by $\Delta\log N = 0.3$–0.8 (i.e. 70–180 per cent). The model stability with respect to observed errors in the value of specific extinction is evaluated by variation of the values of a_V from Table 2 by 0.2 mag kpc^{-1}. According to Section 3 this value can be regarded as the upper limit of error in specific extinction values in our sample. We have found that in this case the model count variations are of the order of $|\Delta\log N| < 0.15$ for all clusters under study.

[4] See the paper by Kilpio & Malkov (1997) for a recent discussion of the extinction formula parameters.

Table 2. Cluster-specific model parameters.

Cluster	l°	b°	a_V (mag kpc^{-1})
Hogg 15	302.0	−0.2	1.00
NGC 2383	235.3	−2.4	0.38
NGC 2384	235.4	−2.4	0.41
NGC 4103	297.6	+1.2	0.59
NGC 4755	303.2	+2.5	0.92
NGC 7510	111.0	+0.1	1.13

In order to estimate the effect of spatial density fluctuations, we consider Galactic spiral arms as the most pronounced Galactic disc substructures. We have carried out model calculations for cluster areas with and without the effects resulting from spiral arms. We considered three local arms (Sagittarius–Carina, Orion and Perseus) represented by logarithmic spirals with parameters taken from Marochnik & Suchkov (1984). It was assumed that the density input from the spiral structure is equal to $\gamma D(R)$, where $D(R)$ is the regular density profile in the disc and γ is a scaling factor taken to be equal to 0.1, 0.2 and 0.3. The model calculations show that, for all clusters in the working magnitude range, the influence of the spiral arms on the stellar density is negligible. The corresponding increase of $\Delta\log N$ is about 0.05 for $\gamma = 0.3$, and less than 0.02 for $\gamma = 0.1$. These values indicate that the effect of density fluctuation is much weaker than that of the extinction.

At last, we compare our model calculations with observed stellar counts in selected stellar fields. Unfortunately, among the clusters of our sample only observations of NGC 2383/4 are supplied with photometry in the blank field containing approximately 300 stars. The field is approximately 5 arcmin away from the clusters and, thus, is partly overlapped with NGC 2383/4 areas (cf. Fig. 2). For model calculations, we use data for this cluster from Table 2. Corresponding distributions are compared in Fig. 3(a). One can observe reasonable qualitative agreement of empirical and model distributions. According to the χ^2 test, both distributions agree at an 80 per cent significance level. A small and generally insignificant excess of brighter stars ($V < 16$ mag) can be attributed to the admixture of NGC 2384 stars.

An excellent opportunity for the verification of our model is provided by wide-field CCD photometry of more than 17 000 stars in the field of NGC 7654, published by Pandey et al. (2001). The photometry covers an area of 40×40 arcmin^2, centred at the cluster with a size of approximately 24 arcsec. This leaves a wide circular blank-field area enabling both the comparison of the model counts and observations, and the estimation of the stochastic variations of circumcluster fields themselves. It is worth noting that NGC 7654 is located only approximately 1° north of NGC 7510, a cluster in the present sample.

In Fig. 3(b) we show observed and model distributions for the NGC 7654 blank-field area. Although Pandey et al. (2001) do not provide an explicit value of the cluster radius, their density profiles show that there is no sufficient cluster population at $r_0 > 13.3$ arcmin. For construction of the observed distribution we use all stars located at $r > r_0$, but the stars from the south-eastern segment of the circumcluster area are not considered. This is where the neighbouring cluster Czernik 43, having a radius of approximately 10 arcmin, is located according to Kharchenko & Piskunov (in preparation). The cluster-specific model parameters ($d = 1380$ pc and $a_V = 1.80$ mag kpc^{-1}) are taken from data for NGC 7654 of Pandey et al. (2001). Because there are indications of an outward increase

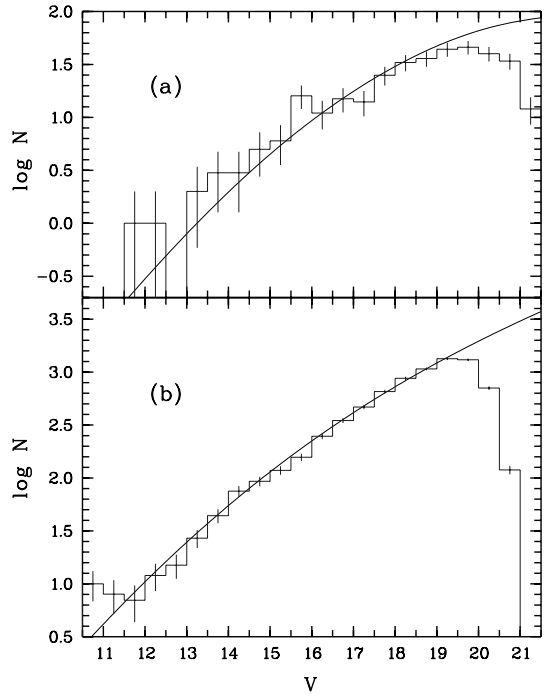

Figure 3. A comparison of stellar counts in test fields, neighbouring the NGC 2383/4 (a) and 7654 (b) clusters, with the predictions of our model. The histograms show empirical data; the bars are the Poisson deviations, indicating data uncertainty. The curves are the model counts.

of the cluster reddening, we use the upper limit provided by the Pandey et al. (2001) values. As one can see from Fig. 3(b), the agreement between the model and observations is good. According to the χ^2 test, both distributions agree at the 90 per cent significance level in the range $V = 12$–19.5 mag. In order to estimate the degree of stochastic variations of circumcluster population, we arbitrarily divide the whole blank field into two equal parts and compared them with the united field separately. The χ^2 test has shown that their statistics are somewhat different: they are the same as the total distribution at the 85 per cent level. This indicates that the model counts approach to member selection is at least not worse than the blank-field method based on an arbitrary sampled test area.

Theoretical differential distributions of stars with apparent magnitude $\psi(V)$, derived with the help of this model, are used for the construction of reduced LFs, as described in Section 4.5.

4.2 Contamination by an overlapping cluster

The contamination by an overlapping cluster is studied using the projected density derived from stellar counts in recent all-sky catalogues. The star counts in the USNO-A2 (Monet et al. 1998) catalogue is strongly affected by crowding effects in the areas of the Hogg 15 and NGC 2383/2384 clusters (which is not surprising for Schmidt camera-based surveys in dense fields). To avoid crowding effects we use the astrograph-based catalogue UCAC1. This catalogue is a part of the all-sky survey UCAC and covers the southern hemisphere south to $\delta_{2000} \approx -20^\circ$ and contains the fields under study.

NGC 2383/2384 lie at the very edge of the UCAC1 survey area, where only short exposures provide star count homogeneity and completeness at $R_u < 13.7$ mag. We construct density profiles in a field centred at NGC 2384. In order to estimate the proper stellar density in a cluster, we count stars in four quadrants separately. The average observed star densities in the field, Σ_f, and in the NGC 2384 corona areas, Σ_{2384}, were determined from the counts in the first and forth quadrants of the corresponding areas located at $\alpha_{2000} \geqslant 7^h.42$ and within $0^\circ.10$–$0^\circ.15$ and $0^\circ.35$–$0^\circ.60$ from the cluster centre, which are free from contamination of NGC 2383 members. As the values of Σ_f and Σ_{2384} do not strongly vary over the studied area, the density of NGC 2383 cluster members can be calculated as $\sigma_{2383} = \Sigma_{2383} - \Sigma_{2384}$ (Σ_{2383} is counted within the NGC 2383 frame). The stellar density of the corona of NGC 2384 itself, therefore, is $\sigma_{2384} = \Sigma_{2384} - \Sigma_f$. The results are shown in Table 3 and one can see that contamination of the NGC 2383 member sample with stars of the NGC 2384 cluster computed as $\sigma_{2384}/\sigma_{2383}$ is approximately 24 per cent.

Table 3. The contributions of field star and neighbouring cluster population are compared with the projected stellar densities of the NGC 2383 and Hogg 15 clusters.

Population	Projected density ($\deg^{-2}$)		Designation
	NGC 2383	Hogg 15	
Observed (total)	2724	6077	$\Sigma_{\rm cluster}$
Field stars	932	1870	$\Sigma_{\rm f}$
Neighbour+field	1273	2401	$\Sigma_{\rm neighbour}$
Neighbour	341	531	$\sigma_{\rm neighbour}$
Cluster	1451	3676	$\sigma_{\rm cluster}$

We cannot estimate the contamination of the NGC 2384 member sample with stars of the NGC 2383 cluster as there are no stars with $R_u < 13.7$ mag within the NGC 2384 frame piece overlapping with the NGC 2383 cluster. Moreover, this frame piece is small and we can assume there are an insignificant number of NGC 2383 members there.

A similar procedure was applied to the Hogg 15 cluster. The counts were performed down to $R_u = 15$ mag. The average observed density in the corona of NGC 4609, Σ_{4609}, was computed from the stellar counts at distance $0^\circ.15$–$0^\circ.20$ and the average observed density of the field stars was computed at $0^\circ.35$–$0^\circ.60$ from the centre of NGC 4609. As one can see from Table 3, Hogg 15 is contaminated with NGC 4609 stars by approximately 14 per cent. This fraction is smaller than in the NGC 2383 case, but it is not negligible.

4.3 Incompleteness effects

It is well known that completeness of a photometric survey is achieved only at approximately 2 mag brighter than $V_{\rm lim}$ (the so-called completeness limit $V_{\rm cmp}$). Below $V_{\rm cmp}$, the observed LF does not reflect the behaviour of a genuine LF and this magnitude range should be excluded from consideration. It is also important to be confident that for clusters with observations in two CCD frames both fields have the same completeness limit. Unfortunately, no $V_{\rm cmp}$ determinations were made in the original papers. This forced us to determine $V_{\rm cmp}$ within this study. Because no test fields were observed in the original papers, we are only able to estimate roughly the completeness limit as a position of the apparent maximum in the distribution of stars with V magnitude within the observed frames. Because the incompleteness increases gradually, the above estimate should be considered as the upper limit of $V_{\rm cmp}$.

The estimated values of $V_{\rm cmp}$ are shown in Table 1. For NGC 4755, we find good agreement between $V_{\rm cmp}$ in both observed frames. Note, however, that the frames do not include the central area of the cluster, containing the brightest cluster members. This causes

another kind of incompleteness, i.e. incompleteness for bright stars. One should keep this in mind when the final result for this cluster is discussed. In contrast, the frames of other clusters are located in central regions and no bright star incompleteness is expected there.

The other kind of incompleteness that should be considered is incompleteness resulting from the overlapping of stellar images in the CCD frame, here called the crowding effect incompleteness (see Sagar & Richtler 1991, for details). It arises as the result of the finite size of stellar images, which depend on stellar brightness. An image of a star of some brightness occupies certain areas within the CCD frame, hides some neighbouring stars of lower brightness and excludes them from the statistics, affecting the brightness function $\psi(V)$, a distribution of stars with apparent magnitude. The relation between the brightness function $\psi_{\rm ce}(V)$, corrected for the crowding effect, and the observed function $\psi_{\rm a}(V)$ is expressed as

$$\psi_{\rm ce}(V) = \psi_{\rm a}(V)\left[1 + \int_{V_{\rm min}}^{V} s(V')\psi_{\rm a}(V')\,{\rm d}V'\right],$$

where the integral represents the necessary correction. Here, $V_{\rm min}$ is the magnitude of the brightest star in the frame, and $s(V)$ is an area occupied in the frame by an image of a star of magnitude V. Both $s(V)$ and $\psi_{\rm ce}(V)$ are expressed in units of the frame area. We have evaluated the crowding effect for each cluster of our sample. The functions $s(V)$ are found empirically for every frame from the image statistics as $s(V) = \pi\, r_{\rm p}^2$, where $r_{\rm p}$ is the average minimum distance in the plane of a frame from stars of magnitude V to the remaining stars. As we found for the considered range of magnitudes, this effect only negligibly (less than 2 per cent) changes the distribution $\psi_{\rm a}(V)$. Thus, we assume $\psi_{\rm ce}(V) = \psi_{\rm a}(V)$ in further discussions.

4.4 Theoretical luminosity functions

For the construction of a theoretical LF $\phi(M_V)$, we have assumed a model of continuous star formation. It is computed as

$$\phi(M_V) = \int_{t_0}^{t_1} \phi_t(M_V)\lambda(t){\rm d}t,$$

where t_0 and t_1 are the minimum and maximum ages of the cluster stars, function $\phi_t(M_V)$, computed using equation (1), is the LF of stars with age t ($t_0 \leqslant t \leqslant t_1$), and λ (t) is the star formation rate (SFR) at age t. The value of t_1, representing the duration since the formation of the first stars, can be regarded as the cluster age.

The mass–absolute-magnitude relation $m(M_V, t)$ and its derivative are calculated along the isochrone of age t using a cubic spline interpolation. For the IMF, we consider a power-law representation $f(m) = km^{-x}$, with k as the normalizing factor and x as the IMF slope to be determined within this study. We assume a constant SFR in our model, $\lambda(t) =$ constant. The resulting parameters for each cluster are drawn from the best fit of the theoretical and observed LFs.

In order to construct theoretical isochrones and LFs that include both post- and pre-MS stages for ages typical of clusters of our sample, we combine the Population I pre-MS evolutionary tracks of D'Antona & Mazitelli (1994) for masses 0.1 to 0.8 $M_\odot$ and Palla & Stahler (1993) for masses 0.8 to 6 $M_\odot$, and Maeder's group post-MS calculations (Schaller et al. 1992) for $m = 0.8$–$120\ M_\odot$. The grids are properly tuned to provide a continuous transition from pre- to post-MS ages and smooth and uniform mass–luminosity and mass–radius relations along the ZAMS. The isochrones are computed from the models corresponding to the Population I chemical abundance $(Y, Z) = (0.30, 0.02)$ using linear interpolation.

In order to convert the theoretical isochrones from the $\log T_{\rm eff}$, $\log L/L_\odot$ plane to the observed $(B-V)_0, M_V$ plane, we use bolometric corrections and $(B-V)_0 - \log T_{\rm eff}$ relations from the Schmidt-Kaler (1982) tables for luminosity classes I, III and V.

4.5 Fitting of theoretical and observed LFs

The following iterative steps are used in the fitting procedure.

(i) Apparent LF construction: the apparent LF (observed brightness distribution) $\psi_{\rm a}$ is constructed from the data available for a given frame(s) as a smoothed density estimation with a rectangular 1 mag wide window and a step of 0.25 mag. The histogram form of the smoothing kernel is selected to apply a correction for field star contamination.

(ii) Construction of a cluster LF: we assume that the apparent LF $\psi_{\rm a}(V)$ is a composition of a distribution of cluster stars with apparent magnitude $\psi_{\rm c}(V)$ and a field star brightness function represented by a Galactic star count model distribution $\psi_{\rm f}(V)$:

$$\psi_{\rm a}(V) = \psi_{\rm c}(V) + p\psi_{\rm f}(V),$$

where the free parameter p denotes the percentage of field stars contaminating the sample. With the help of the apparent distance modulus $V - M_V$, the function $\psi_{\rm c}$ is transformed to the absolute magnitude scale and hereafter is called the observed cluster LF $\phi_{\rm c}(M_V)$.

(iii) Luminosity function fitting: the theoretical LF $\phi(M_V)$, smoothed in the same way as the observed LF, is fitted to the empirical function $\phi_{\rm c}(M_V)$ within a cluster-specific range of magnitudes. The entropy

$$\Delta = \sum \left|\phi_{\rm c}\left(M_V^i\right)\log\left[\phi_{\rm c}\left(M_V^i\right)/\phi\left(M_V^i\right)\right]\right|$$

is constructed to find the best-fitting parameters $\{p, x, t_0, t_1\}$.

Steps (ii) and (iii) are repeated iteratively by varying p until the best agreement (in terms of χ^2 statistics) between theoretical and observed LFs is achieved. The parameter p is varied between 0 and 1 in a step of 0.1.

Internal accuracy of x, $\log t \equiv \log t_1$ and $\Delta\log t \equiv \log t_1 - \log t_0$ is estimated on the basis of the kernel smoothing theory (Silverman 1986; Lapko et al. 1996) for selected histogram grid parameters (range and step). The accuracy of the field star percentage p is estimated from

$$\sigma_{\rm p}^2 = \frac{\sum(p_i - \overline{p})^2/\chi_i^2}{\sum 1/\chi_i^2}, \quad \overline{p} = \frac{\sum p_i/\chi_i^2}{\sum 1/\chi_i^2},$$

assuming that $\sigma_{\rm p}^2$ is a second-order central moment of a distribution function equal to that of $1/\chi^2$.

5 DISCUSSION

The results of the LF fitting are listed in Table 4. For each cluster we show fit parameters. These are the range of absolute magnitudes selected for the LF fit; the best-fitting χ^2 value achieved in the iterations and derived parameters; the position of the H-maximum in the theoretical LF $M_V^{\rm H}$, indicating the absolute magnitude of the turn-on point; the derived percentage of the field star contamination p; the IMF slope x; the adopted age of a cluster $\log t$; and the age spread parameter $\Delta\log t$. Note that parameter errors shown in Table 4 are in good agreement with the uncertainty estimates given in Section 3 on the basis of data accuracy analysis. The results are discussed separately below for the clusters under study.

Table 4. Open cluster parameters derived from the fit of the LFs.

Cluster	Fit parameters			Derived parameters			
	M_V range (mag)	χ^2	M_V^H (mag)	p	x	$\log t$	$\Delta\log t$
NGC 2383	−6.0, 3.0	23.6	2.50	0.1 ± 0.2	2.2 ± 0.4	7.1 ± 0.2	0.0 ± 0.2
NGC 2383[a]	−2.0, 3.0	37.2	–	0.2 ± 0.2	1.2 ± 0.4	8.5	–
NGC 2384	−5.0, 3.0	39.6	2.00	0.3 ± 0.2	1.0 ± 0.5	7.0 ± 0.2	0.2 ± 0.4
NGC 2384[b]	−5.0, 3.0	41.5	2.00	0.2 ± 0.2	1.0 ± 0.5	7.0 ± 0.2	0.2 ± 0.4
NGC 4103	−3.5, 2.0	24.1	1.25	0.3 ± 0.2	1.5 ± 0.6	6.8 ± 0.1	0.2 ± 0.4
Hogg 15	−5.0, 2.5	79.2	0.75	0.6 ± 0.2	1.3 ± 0.4	6.7 ± 0.3	0.6 ± 0.6
Hogg 15[c]	−5.0, 2.5	17.0	0.75	0.5 ± 0.2	1.3 ± 0.4	6.6 ± 0.3	0.2 ± 0.6
NGC 4755	−3.0, 3.0	10.8	2.50	0.2 ± 0.2	1.4 ± 0.3	7.2 ± 0.2	0.2 ± 0.2
NGC 7510	−6.0, 1.5	13.8	0.75	0.3 ± 0.2	1.2 ± 0.4	6.8 ± 0.3	0.5 ± 0.7

[a]Corrected for contamination by NGC 2384 stars, $\log t = 8.5$ is accepted from the upper MS isochrone fitting.
[b]Derived in the frame area free from NGC 2383 stars.
[c]Corrected for contamination by NGC 4609 stars.

In Fig. 4, we show the CMDs of clusters under discussion. The reddening and distance parameters are taken from Table 1 and fine-tuned by the variation of the tabular values within their accuracy to reach the best agreement of the cluster CMD, empirical ZAMS and corresponding isochrones. Cluster proper motion members and non-members are marked if cluster stars are bright enough to be included in the ASCC-2.5. To give an idea how the adopted distances and reddening values agree with the photometry, in Fig. 4 we show the position of the empirical ZAMS of Schmidt-Kaler (1982). In order to illustrate how ages derived from the LF analyses conform with cluster CMDs, in Fig. 4 we also show the isochrones corresponding to the ages, t_0 and t_1.

In Fig. 5, we display the LFs. The observed cluster LF ϕ_c, constructed as described in Section 4.5, is shown with filled histogram, and the corresponding theoretical LF ϕ fitted to ϕ_c is shown with a curve (the fitted portion of ϕ is shown with a heavy curve, while the rest is marked with a thin curve). For the purposes of comparison, we also show the apparent LFs ψ_a (thin histogram and hatched area) and the contribution from field stars ψ_f (dotted curve), both displaced by the value of $V - M_V$. Below we discuss each cluster as per their appearance in Figs 4 and 5.

5.1 Hogg 15

In the cluster CMD, one can indicate the MS turn-on point at $M_V^* \approx 0.5$ mag. Note that the H-feature should also be found in the LF in the vicinity of M_V^*, where the apparent LF of Hogg 15 stars also shows a local maximum. The data incompleteness dominates after $M_V = 3$ mag, where ψ_a gradually decreases in agreement with Table 1, indicating that $M_V^{cmp} = 3.1$ mag. The field star contamination for Hogg 15 is found to be highest amongst clusters considered here. This effect, as is seen from the filled histogram in Fig 5, keeps the LF practically unchanged in the brighter portion ($M_V < 0.5$ mag), and hides the H-feature region substantially.

In order to take into account contamination from an overlapping cluster NGC 4609, the theoretical LF $\phi(M_V)$ was composed of two populations belonging to these clusters. Because the clusters reside at different distances from the Sun, the stars of NGC 4609 should be shifted with respect to that of Hogg 15 by the difference of the cluster apparent distance moduli $\Delta(V - M_V)$. Because $V - M_V$ of NGC 4609 is equal to 11.45 mag according to LGM2.2, the value of $\Delta(V - M_V)$ is taken to be equal to −5.05 mag. As a result of a small fraction of NGC 4609 stars projected on to the Hogg 15 area (approximately 15 per cent of the Hogg 15 population according to Section 4.2), the specific shape of the corresponding mass spectrum is not important and we assume that it follows the Salpeter law. The age of NGC 4609 is taken from Mermilliod (1981) as $\log t = 7.56$. A composite LF is shown in Fig. 5 with a solid curve, while the input from the NGC 4609 population is shown with a dot–dashed curve.

As one can see from Table 4, taking into account the population of NGC 4609 does not strongly change the cluster parameters (except the age spread), but it considerably improves agreement between theoretical and observed parameters, notably reducing the χ^2 parameter.

Fig. 4 shows that ages t_0, t_1 derived from the LF fitting are in good agreement with the cluster CMD. The observed cluster LF ϕ_c also demonstrates a high degree of conformity with the composite theoretical LF. A deep and narrow gap of ϕ_c at approximately $M_V \approx 2$ mag shows that the derived input of field stars p is somewhat overestimated. As shown in Table 4, Hogg 15 is one of the two clusters in our sample where considerable (although quite uncertain) age spread of $\Delta\log t = 0.6$ is detected. This value, however, is reduced to the insignificant value of $\Delta\log t = 0.2$, which is common to the whole sample, if one takes into account the contamination from NGC 4609. We therefore conclude that the age spread in Hogg 15 is introduced mainly as a result of the admixture of field and overlapping neighbouring stars, and consider the cluster parameters as derived for the Hogg 15[c] case.

Hogg 15 is the youngest cluster of our sample, with an age of 4 Myr. How does this value compare with the earlier published values? Originally, the age of Hogg 15 was estimated by Moffat (1974) as 8 Myr. According to Lyngå (1987), the age is 10 Myr. Recent values come generally from isochrone fitting of the upper MS: LGM2.2 define it as 6 Myr; Sagar et al. (2001) provide an age estimate of 6 ± 2 Myr; Piatti & Clariá (2001), who initially found it to be 300 Myr, later reduced this unusually high value to 20 ± 10 Myr (Piatti et al. 2002). The technique of matching integrated theoretical and observed spectra of the cluster led Ahumada et al. (2000) to suggest age values of 5 ± 2 or 30 Myr. Because MS turn-off ages are biased toward higher values, our age estimate, based on the MS turn-on point technique, is in fact the lowest one. Note, however, that the majority of the above-mentioned values agree with the present one within their accuracy. The IMF slope was determined for Hogg 15 stars by Sagar et al. (2001), who found it to be equal 1.35 ± 0.21, which again coincides with the present result.

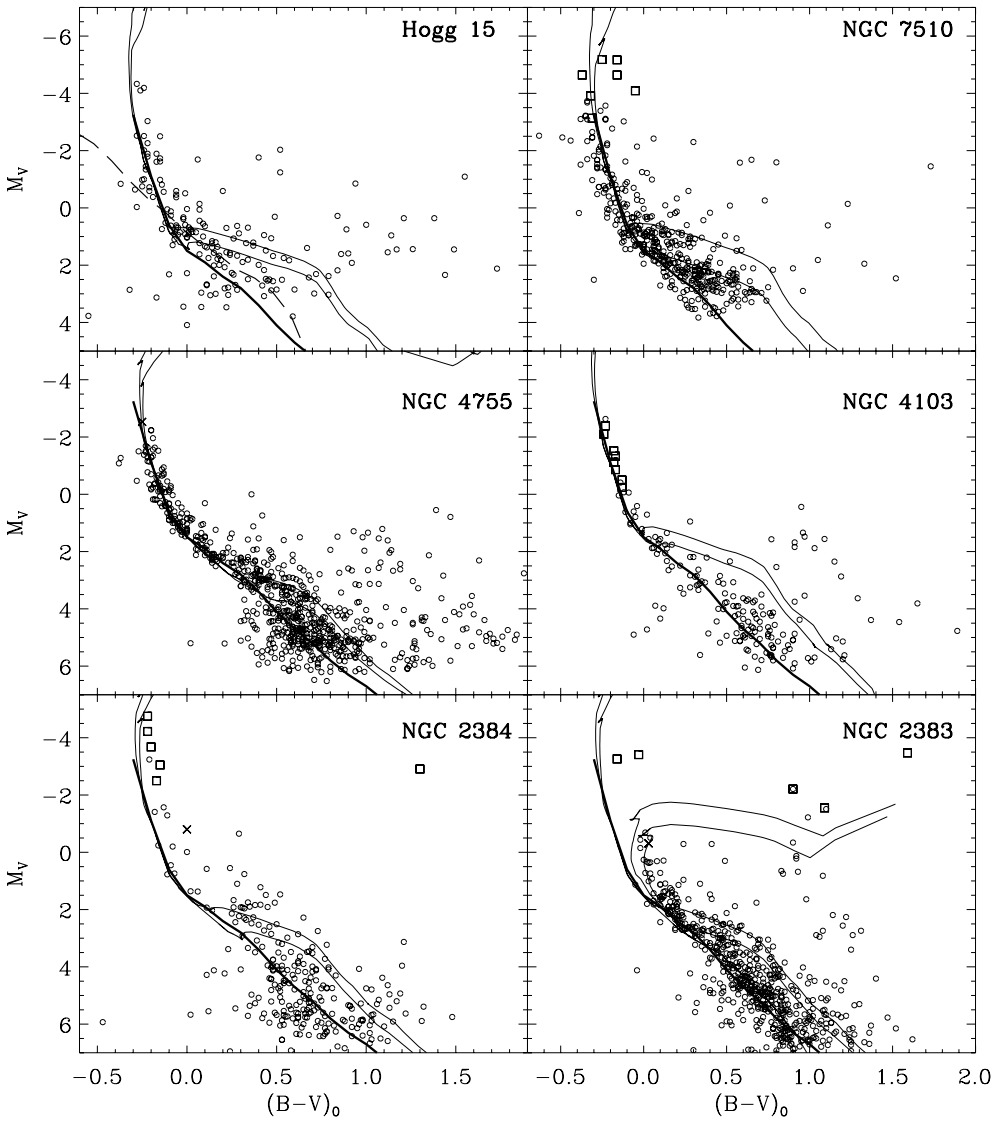

Figure 4. Colour–magnitude diagrams of studied clusters. Open circles are stars from original observations corrected for adopted $V - M_V$ and $E(B - V)$ values. Squares and crosses are proper motion cluster members and field stars, respectively, from ASCC-2.5. The heavy curve is an empirical ZAMS of Schmidt-Kaler (1982), and the lower and upper thin curves are isochrones corresponding to derived age parameters t_1 and t_0, respectively. For NGC 2383, we show for comparison both isochrones of $\log t = 8.3$ and 8.5, fitted to its upper MS, and isochrones of $\log t = 6.8$ and 7.0, corresponding to age parameters of NGC 2384, derived from the analysis of its LF. For Hogg 15, we show corresponding isochrones as listed in Table 4. The long-dashed curve is the MS of NGC 4609 as it would appear for the Hogg 15 reddening and distance.

5.2 NGC 7510

It can be seen from the CMD that the regular cluster sequences are embedded in a cloud of, presumably, field stars. The astrometric members also show definite spread around the MS turn-off point. It may be that some of them are comoving field stars. The MS turn-on point can be detected somewhere between $M_V^* \approx 0.5$ and 1.5 mag. The apparent LF ψ_a shows a broad plateau between $M_V^* \approx 0.5$ and 3 mag, with a weak maximum at $M_V = 2.25$ mag. As indicated by Galactic model star counts, it should be formed mostly by field stars. The sample demonstrates certain incompleteness below the maximum, where ψ_a, instead of a steady increase, slowly falls. According to Table 1 the completeness limit of original data is $M_V^{\rm cmp} = 0.9$ mag. We select $M_V = 1.5$ mag as a faint limit of the LF fitting range based on the value of the χ^2 parameter. The agreement between observed cluster LF ψ_c and theoretical LF is one of the best amongst the studied clusters.

As one can see from Fig. 4, the ages $t_0 = 2$ and $t_1 = 6$ Myr, derived from the LF fitting, are in good agreement with details of the cluster CMD. The lower pre-MS branch of the cluster coincides with the t_1 isochrone. The t_0 isochrone fits the apparent sequence of stars deviating from the MS at $M_V \approx 1$ mag. Stars forming this group do not show evident concentration to the cluster centre. If, however, this group is not a random concentration of field stars, one can regard this as an evidence of the second star formation event in the cluster.

Excellent agreement between theoretical and observed LFs concerns only the MS. We are unable to follow the H-feature over its full width and are not certain if the descending portion of the ψ_c is related to this detail or is a consequence of the data incompleteness of

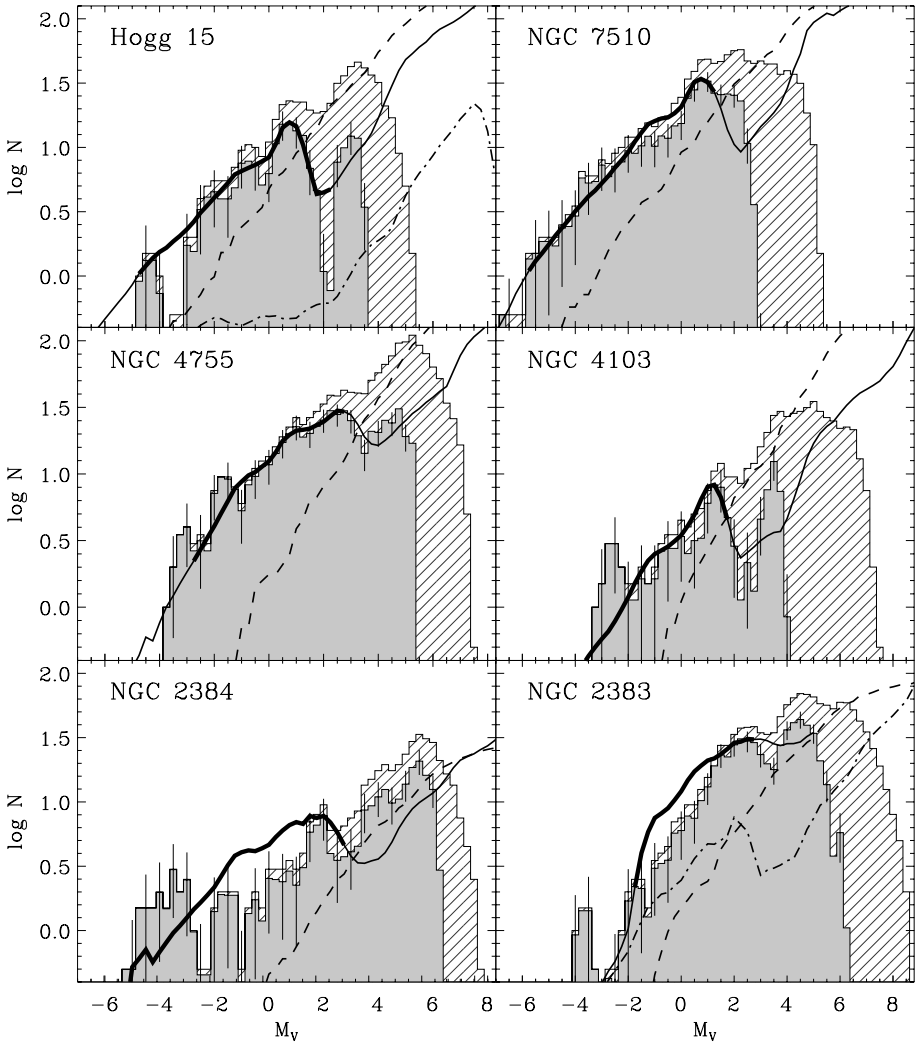

Figure 5. Luminosity functions of the clusters under study. Histograms show observed LFs: an apparent LF $\psi_a(M_V)$ (hatched) and cluster star LF $\phi_c(M_V)$ corrected for the effect of field stars (filled); bars are Poisson deviations indicating data uncertainties. Curves are theoretical LFs: cluster star LF $\phi(M_V)$ fitted to $\phi_c(M_V)$ (solid) and field star brightness function $\psi(V)$ displaced along the abscissa by $V - M_V$ (dashed). The heavy portion of the theoretical LF marks the range of fitting. For Hogg 15 and NGC 2383, solid curves show composite LFs, which take into account the influence of a neighbour, and dash-dotted curves show the model LF, which mimics the neighbouring cluster star population (see Sections 5.1 and 5.5 for details).

the present survey. Note, however, that the cluster age derived from the assumption that the H-maximum is located at $M_V \approx 1$ mag (just coinciding with the data completeness limit) is in agreement with the CMD arguments, which are independent of data incompleteness. In contrast, the mass spectrum slope found from the brighter portion of the LF should be regarded as a confident one.

The MS turn-off age of NGC 7510 can be found in the Lyngå (1987) catalogue (10 Myr) and in the LGM2.2 list (38 ± 2 Myr). Sagar & Griffiths (1991) find the age to be <10 Myr. Again, our age of 6 Myr is the lowest estimate of these values. The mass function of stars of NGC 7510 was constructed by Sagar & Griffiths (1998). It was found that in the mass range 1–14 $M_\odot$ the mass function slope x is 1.1 ± 0.2, which again fits present results well.

5.3 NGC 4755

NGC 4755 is the only cluster of our sample that is observed in two frames, located on both sides of the dense cluster centre (Fig. 2). We find that both the frames are similar with respect to photometric quality and the completeness issue, sowe consider them together.

The cluster CMD shows well-defined stellar sequences. The MS turn-on point can be seen at $M_V^* \approx 3$ mag and, correspondingly, the H-feature is expected to be located at $M_V = 3$ mag and fainter. The uncorrected LF ψ_a shows a step at $M_V = 2$–3 mag, related to the cluster H-feature. The data incompleteness dominates after $M_V =$ 5.5 mag (5.2 mag according to Table 1), where ψ_a gradually falls. Correction for field stars for this cluster can be made with a certain confidence. By comparison with the model brightness function ψ_f, it can be seen that at brighter magnitudes the incompleteness can be regarded as negligible. Thus, selecting $M_V = 3$ mag as a faint limit for the LF fitting range, we are safe from the data incompleteness bias. Because the brightest stars, residing in the cluster centre and shown in Fig. 5, are not present in original data (see Fig. 4), we select $M_V = -3$ mag as the bright limit of the fitting range. As is seen from the filled histogram of Fig. 5, we correctly identify the H-maximum position and, in spite of the fact that the fitting was made only for the MS portion of the LFs, the theoretical LF reproduces

well the pre-MS H-feature after LF reaches its minimum and turns over again. However, we are not able to reach the convective portion of the LF as a result of the relatively brighter completeness limit of the present data.

It is seen that the theoretical LF is in good agreement with the observed one, ϕ_c, even outside the fitting range. The derived age spread of cluster stars, according to Table 4, is insignificant and we conclude that no evidence of continuous star formation can be found from the LF analysis for this cluster. As one can see from Fig. 4, the age of 16 Myr as derived from the LF fitting technique is in good agreement with the cluster CMD. The IMF slope coincides within its accuracy with the Salpeter value.

The MS turn-off age of NGC 4755 can be found in the Lyngå (1987) catalogue (7 or 24 Myr) and in the LGM2.2 list (16 ± 3 Myr). Sagar & Cannon (1995) find that it is approximately 10 Myr and most pre-MS stars have ages between 3 and 10 Myr. The recent age estimation of 10 ± 5 Myr, derived from the fitting of the upper MS, is given by Sanner et al. (2001). For this particular cluster our age estimate of 16 Myr is close to an average of previously published values. The mass function of the NGC 4755 stars was constructed by Sanner et al. (2001). It was found that in the mass range 1–13 $M_\odot$ the slope x is 1.68 ± 0.14, which is significantly steeper than the value estimated here.

5.4 NGC 4103

The observed frame (see Fig. 2) covers only a minor part of the cluster centre. One can, therefore, expect the results to be more uncertain in comparison with the majority of other clusters under study.

In the cluster CMD, the MS turn-on point can be seen at $M_V^* \approx 1.75$ mag and the H-feature dip is expected at $M_V = 2$–4 mag, seen as the CMD area of lower density. The apparent LF ψ_a shows a weak local maximum at $M_V = 1.5$ mag. The data incompleteness (see Table 1) dominates at $M_V > 4.8$ mag, where ψ_a gradually falls. However, ψ_a flattens after $M_V = 4$ mag, which indicates the existence of certain data incompleteness at brighter magnitudes. To be completely safe against this effect and taking into account the fact that the shape of ψ_a at $M_V = 2.5$–3.5 mag is very close to that of the model field star brightness function, indicating a high fraction of field stars in this magnitude range, we select $M_V = 2$ mag as a faint limit of the LF fitting range. The minimum of χ^2 is achieved at $p = 0.3$, with the corresponding parameters shown in Table 4.

In spite of the cluster LF ϕ_c starting to increase after $M_V \approx 3$ mag, we cannot regard the H-feature with the same confidence as in Hogg 15 or NGC 4755 because of poor statistics. It should be noted, however, that, as in the case of NGC 4755, the theoretical LF, being fitted to the MS observations, reproduces the empirical pre-MS stage reasonably well. The cluster age, derived from the LF and MS turn-on point analysis, shows that this cluster seems to be generally younger than it was considered to be before, from the MS turn-off dating technique (see below). It should be noted, however, that NGC 4103 is the case where the MS turn-off technique resulting from the practically unevolved upper MS of the cluster is able to provide an upper age estimate only. In contrast, the mass spectrum slope, found from the brighter portion of the LF, should be regarded as accurate enough. Note some excess of the brightest stars ($M_V \approx -3$ mag), which, however, can be a consequence of random placement of rare bright field stars over the cluster region.

All the authors provide an NGC 4103 MS turn-off age and are unanimous in its value. The age is 22–41 Myr according to Lyngå (1987), and 24 ± 9 Myr according to LGM2.2. Sagar & Cannon (1997) find it to be approximately 30 Myr, Forbes (1996) estimated approximately 25 Myr and notes that the MS turn-on age should not be much different, and according to Sanner et al. (2001) the age is 20 ± 5 Myr. Again we give the lowest value of the cluster age of approximately 6 Myr, and believe that both cluster CMD and LF support this value. The mass function of stars of NGC 4103 was constructed by Sanner et al. (2001). It was found that in the mass range 0.7–12 $M_\odot$ the slope x is 1.46 ± 0.22. Almost the same value is estimated here.

5.5 NGC 2383 and 2384

In the NGC 2383/2384 pair, the dominating role in the neighbour contamination is played by the extended and loose cluster NGC 2384 (see Sections 4.1 and 4.2). In contrast, the central part of NGC 2384 can be regarded as relatively free from the influence of NGC 2383. Therefore, we start this section with a discussion of the NGC 2384 results.

The CMD of NGC 2384 in its lower part is very fuzzy, while the MS part of the diagram is well defined. Subramaniam & Sagar (1999) even assume that stars fainter than $V = 16$ ($M_V = 2.8$) mag are mainly field stars, as can be seen from Fig. 4. Nevertheless, a certain fraction of cluster members is observed even at the faintest magnitudes. These are pre-MS stars, forming the upper bound of the observed sequence at $M_V > 2$ mag. In contrast to other clusters, the CMD of NGC 2384 does not display an extended halo of field stars, where cluster MS and pre-MS sequences are embedded. Field stars (presumably giants and late type dwarfs) form a compact clump in the bottom of the diagram, with $(B-V)_0 \approx 0.6$ mag and $M_V \gtrsim 4$ mag, leaving the Hertzsprung gap to be unoccupied. The MS turn-on point in the CMD is less certain than for other clusters. If one correlates cluster CMD with the morphology of the observed LF, one should detect it around $M_V^* = 2 - 2.5$ mag, where cluster MS stars certainly cease to appear, and simultaneously a local detail resembling the H-feature appears in the observed LF. One can observe, however, that a few of the pre-MS stars do appear in the CMD at brighter magnitudes ($M_V \approx 0.5$–1.5 mag). Their extension forms an upper bound of a broad pre-MS branch, extending down to the limit of observations. The regularity of this feature implies that it is not a random pattern of field stars. They would be rather unresolved pre-MS binaries, or the youngest generation of NGC 2384 stars. Note, however, that this brighter position of the MS turn-on point does not produce anything resembling the H-maximum, expected to be located near this point (see Section 2).

The LF of NGC 2384 demonstrates irregular behaviour and its agreement with the theoretical LF is worse in comparison with the other clusters under study. This is confirmed statistically because the χ^2 value is highest for this cluster (except for the Hogg 15 case with no correction for contamination by NGC 4609). One can mention an excess of observed numbers of massive stars ($M_V \approx -4$ mag), and a deficiency of medium-mass stars ($M_V = -1 \ldots +1$ mag) with respect to the theoretical LF ϕ. Also, the LF detail, which we identify with the H-feature, is poorly developed: the observed H-dip is narrower than the theoretical one. This behaviour conforms with the mass segregation scenario in the case of the observed frame covering the central part of the cluster only. The derived slope of the mass function is similar to values found by de Grijs et al. (2002b) for the central parts of the rich LMC clusters NGC 1805 and 1818. The LF irregularity could, therefore, be attributed to incomplete member statistics. The greater extent of the cluster compared with the observed frame naturally explains other peculiarities of the NGC 2383/4 pair, such as the presence of early-type stars in the NGC 2383

field and the existence of the underdeveloped H-feature in its LF (see below), or the weak excess of bright stars in the neighbouring blank field (see. Section 4.1).

The stability of the NGC 2384 parameters against the contaminating effect of NGC 2383 was checked using data from part of the NGC 2384 frame located outside the NGC 2383 area (see Fig. 2). As one can see from Table 4, there is no difference between the derived parameters of NGC 2384 in both cases. Thus, we can regard the influence of the NGC 2383 member contamination on the derived parameters of NGC 2384 to be negligible.

The colour–magnitude diagram of NGC 2383 is more populated than that of the neighbouring NGC 2384. There is a well-defined evolved portion of the MS compatible with cluster age $\log t = 8.5$, which is in agreement with an estimate of $\log t = 8.45$–8.6 by Subramaniam & Sagar (1999) and differs from the ages $\log t = 7.4$ and 7.17 derived by Lyngå (1987) and LGM2.2, respectively. This contradiction arises as a result of the presence of bright ASCC-2.5 kinematic members with ages of a few tens of Myr. The MS turn-on point, corresponding to this younger age, cannot be easily identified in the CMD. Nevertheless, the LF indicates the presence of the H-detail even in the apparent LF $\psi_{\rm a}$. The MS-band at fainter magnitudes ($M_V \gtrsim 2$ mag) is widened and, unlike the other clusters studied here, it is not caused by field giants extending the MS from the side of fainter magnitudes, but it is the result of bright stars forming the high-luminosity envelope of the MS.

In the corrected LF $\phi_{\rm c}$, the H-feature becomes more pronounced, leaving the H-dip to be somewhat underdeveloped (more shallow and narrower than in the corresponding theoretical LF), however. The cluster age derived from the LF fitting corresponds to a lower age estimate coming from the brightest MS stars. The value of χ^2 indicates that the LF fit is more reliable than in the case of NGC 2384. Note the unusually steep value of the IMF slope $x = 2.2$ estimated for this cluster. In spite of formally satisfactory results of the LF fitting, there are several points indicating that NGC 2383 carries signs of a dual nature, which were not taken into consideration. For example, the evolved upper MS indicates that NGC 2383 is approximately 300 Myr old (see Fig. 4), while the LF indicates that its age is close to that of NGC 2384. The relatively young age of NGC 2383 is also supported by the presence of bright MS kinematic members. Possibly, this is the main reason for assigning a younger age to the cluster by Lyngå (1987) and LGM2.2. This confusion can be removed with the help of a model of an overlapping neighbour, with the only difference from the case of Hogg 15 being that in this case the degree of contamination with NGC 2384 stars is higher (see Section 4.2). This is also supported by the independent data of the ASCC-2.5, which indicate that these clusters are not only located close together in the sky, but also have similar proper motions (see Kharchenko et al.). So a probable proper motion member of one cluster may well also belong to the other, and the brightest kinematic members of NGC 2383 could be actually projected members of NGC 2384. This can also be supported by the fact that numerous MS stars of NGC 2383 forming the upper envelope at $M_V \gtrsim 2$ mag could actually be pre-MS stars of NGC 2384. Apart from the coincidence with the positions of corresponding isochrones in the CMD, this idea is also supported by the spatial distribution of these stars. They tend to be located in the NGC 2383 frame within the circle of its neighbour. The number of these stars is compatible with the degree of contamination derived from stellar counts, and they might be responsible for the steeper IMF slope found for NGC 2383, when neglecting the influence of NGC 2384.

In order to take into account contamination from the overlapping cluster theoretical LF of NGC 2383, $\phi(M_V)$ was composed of two populations belonging to both clusters. Unlike the case of Hogg 15, NGC 2383 and 2384 reside at the same distance within the errors [$\Delta(V - M_V) = 0.1$–0.3 mag]. So no correction is required for the LF magnitude scale while constructing the composed theoretical LF. We assume that the mass spectrum of NGC 2384 stars does not vary with location and the case of NGC 2384^b in Table 4 can be considered because it is representative. The corresponding values of t_0 and t_1 are also taken from Table 4. Because no developed H-feature exists in the LF at $t \sim 300$ Myr, we are forced to use the LF of NGC 2383 in a customary way, i.e. for determination of x and p parameters. The cluster age is found from the MS turn-off point and fine tuned to satisfy the χ^2 test. The lowest χ^2 value is achieved at $\log t = 8.3$, which is somewhat less than isochronic age of $\log t = 8.5$ (Fig. 4), determined from the post-MS isochrone fitting. As a result of the above-mentioned reasons, we regard this disagreement as insignificant and show in the turn-off age in Table 4. The best-fitting composite LF for the NGC 2383^a case is shown in Fig. 5 with a solid curve, while the contaminating model LF of NGC 2384 is shown with the dash–dotted curve.

As one can see from Table 4, the proposed model provides a less accurate fit of the theoretical LF to the observed LF than the previous one. On the other hand, it harmonizes the full observation scope (star counts, cluster CMDs and LFs). As a result, with the age determined from the MS turn-off point calibration, the IMF slope has been reduced to a value close to the Salpeter one with the value of p almost unchanged.

In the light of the above discussions, it is not surprising that the cluster parameters derived in the present study are in good agreement with those derived in the original paper by Subramaniam & Sagar (1999). For example, our values of x practically coincide with those of Subramaniam & Sagar (1999), who found $x = 1.3 \pm 0.15$ for NGC 2383 and $x = 1.0 \pm 0.15$ for NGC 2384. Similarly, in agreement with Subramaniam & Sagar (1999), we consider that the NGC 2383 ages listed by Lyngå (1987) as 25–41 Myr or by LGM2.2 as 16 Myr are underestimated, while the NGC 2384 ages [1–10 Myr according to Lyngå (1987) and 8 ± 1 Myr according to LGM2.2] are in fair agreement with our result. However, again, the age of NGC 2384 derived from LF fitting is lower than that derived by Subramaniam & Sagar (1999) from the upper part of the MS.

Subramaniam & Sagar (1999) conclude that, in spite of their spatial proximity, the clusters NGC 2383/2384 do not constitute a physical pair in the sense of a common origin. The present study not only supports this point, but also it makes it stronger. In spite of the fact that both clusters do overlap in the plane of the sky where they reside approximately at the same distance from the Sun and have similar proper motions, they are very different in all other respects, e.g. cluster geometry, morphology, environment, stellar contents, and age, and cannot be regarded as twins.

6 CONCLUSIONS

The major aim of the present study was to elaborate tools, which provide a comprehensive investigation of remote young open star clusters having accurate CCD photometry. The effort was focused on revealing the main-sequence turn-on areas, important from the point of view of both young cluster dating and luminosity and mass function analysis. To enable the statistical selection of cluster members for a vast set of open cluster CCD observations with no data on adjacent blank fields, and thus to involve them in luminosity and mass function studies, we have proposed a new approach to the field star removal technique based on the use of a Galactic disc star count model. As we found, as a result of high confidence in interstellar

extinction determination, open clusters are especially suitable objects for this technique, providing selection results at least of the same quality as the standard method of blank fields. The proposed approach could be especially valuable for deep observations of young clusters, planned to be observed in the framework of present-day surveys (see e.g. Kalirai et al. 2001), which are able not only to reach turn-on regions of selected young clusters, but also to reveal complete H-details down to convective portions of luminosity functions.

The main conclusion from the present study of the six such clusters residing at heliocentric distances of 2–4 kpc is that their CCD observations, coupled with the Galactic model star counts, wide-area statistics provided by all-sky catalogues and theoretical LFs fitted to the observations, are sufficient to study their population, construction of detailed luminosity and mass functions and age, provided the photometry is deep enough to reach the LF H-feature. The direct comparison of observed and theoretical LFs, instead of converting them to stellar mass spectra, is of principal importance in this approach. It provides a standard candle, which can be used for reliable cluster dating. Otherwise, this is very difficult because the upper MS of young clusters usually implemented for this aim is too steep and the degree of stellar evolution is, as a rule, too insignificant to provide reliable cluster ages: in fact, it only provides upper estimates for the cluster age. The main conclusions can be written as follows.

(i) Contamination of cluster members with field stars is the most important factor influencing the lower part of the cluster CMD and LF. For the clusters under study, field star contamination varies in the range of 20–50 per cent.

(ii) The overlapping clusters may considerably distort the observed LFs. The neighbour contamination, in addition to field stars, is equal to 14 per cent in the case of Hogg 15 and 24 per cent in the case of NGC 2383.

(iii) The LF H-feature was found well beyond statistical noise in all the clusters under study. For most of the clusters, its location agrees well with the theoretical prediction. We believe that in the case of NGC 2384, where the H-feature displays an underdeveloped structure, this can be explained by the complexity of the area and spatial incompleteness of the data. The false H-feature observed in NGC 2383, which certainly is too old to be demonstrated, is the result of contamination of the cluster field with NGC 2384 stars.

(iv) Cluster ages derived in the present study are, as a rule, several times lower than those determined from the fitting of the theoretical isochrones to the turn-off parts of the MS. We believe that our ages are more accurate than those derived from the upper MS. Note that, although we used a continuous star formation model, the derived durations of star formation events only insignificantly differ from zero.

(v) Stellar mass spectra of studied clusters are well represented with a power law with slopes which as a rule agree with the Salpeter value, within errors. One should keep in mind, however, that because the observed data concern the central parts of clusters, the derived mass spectra might be different from the IMF because of the mass segregation effect. The unusually flat mass function of NGC 2384 can be treated, for example, as indirect evidence of the higher extent of this cluster and the presence of the mass segregation effect.

ACKNOWLEDGMENTS

The authors thank the anonymous referee for useful comments. This work was partly supported by RFBR grant No. 01-02-16306. AEP is grateful to the Indian National Science Academy, New Delhi, for funding the visit to India in the autumn of 2000, when this work was initiated. ANB acknowledges the financial support of the INTAS (grant INTAS YSF 00-152).

REFERENCES

Ahumada A. V., Claria J. J., Bica E., Piatti, A. E., 2000, A&AS, 141, 79
Andrievsky S. M., Bersier D., Kovtyukh V. V., Luck R. E., Maciel W. J., Lépine J. R., Beletsky Yu. V., 2002, A&A, 384, 140
Bahcall J. N., 1986, ARA&A, 24, 577
Belikov A. N., 1999, PhD thesis MSU, Moscow
Belikov A. N., Piskunov A. E., 1997, Astron. Rep., 41, 28
Belikov A. N., Hirte S., Meusinger H., Piskunov A. E., Schilbach E., 1998, A&A, 332, 575
Da Costa G. S., 1982, AJ, 87, 990
D'Antona F., Mazitelli I., 1994, ApJS, 90, 467
de Grijs R., Johnson R. A., Gilmore G. F., Frayn C. M., 2002a, MNRAS, 331, 228
de Grijs R., Gilmore G. F., Johnson R. A., Mackey A. D., 2002b, MNRAS, 331, 245
de Grijs R., Gilmore G. F., Mackey A. D., Wilkinson M. I., Beaulieu S. F., Johnson R. A., Santiago B. X., 2002c, MNRAS, 337, 597
Dias W. S., Lépine J. R. D., Alessi B. S., 2002, A&A, 389, 871
Forbes D., 1996, J. R. Astron. Soc. Can., 90, 329
Gilmore G., 1984, MNRAS, 207, 223
Holmberg J., Flinn C., Lindengren L., 1997, in Battrick B., ed., ESA, *Hipparcos* Venice'97 Symp. ESA Publications, Noordwijk, p. 721
Jahreiß H., Wielen R., 1997, in Battrick B., ed., ESA, *Hipparcos* Venice'97 Symp. ESA Publications, Noordwijk, p. 675
Kalirai J. S. et al., 2001, AJ, 122, 257
Kharchenko N. V., 2001, Kinematics Phys. Celest. Bodies, 17, 409
Kharchenko N., Schilbach E., 1996, Baltic Astron., 5, 337
Kharchenko N., Rybka S., Yatsenko A., Schilbach E., 1997, Astron. Nachr., 318, 163
Kharchenko N. V., Pakulyak L. K., Piskunov A. E., 2003, AZh, 80, 291
Kilpio E. Yu., Malkov O. Yu., 1997, AZh, 74, 15
Kislyuk V., Yatsenko A., Ivanov G., Pakulyak L., Sergeeva T., 1999, in Soffel M., Capitaine N., eds, Proc. IX Lohrmann Coll., Systèmes de Référence Spatio-temporales. Obs de Paris Publ., Paris, p. 61
Lapko A. V., Chentzov S. V., Krokhov S. I., Feldman L. A., 1996, Self-Leaning Systems of Data Processing and Decision-Making. Nonparametric Approach, Nauka, Novosibirsk
Loktin A. V., Gerasimenko T. P., Malysheva L. K., 2001, Homogeneous Catalogue of Open Cluster Parameters, Release 2.2 (see also the WEBDA data base at http://obswww.unige.ch/webda/) (LGM2.2)
Lyngå G., 1987, Catalogue of Open Cluster Data, 5th edn, S7041. Centre de Données Stellaires, Strasbourg
Marochnik L. S., Suchkov A. A., 1984, The Milky Way Galaxy. Nauka Publications, Moscow
Mermilliod J.-C., 1981, A&A, 97, 235
Moffat A. F. J., 1974, A&A, 34, 29
Monet D. et al., USNO-A 2.0: A Catalog of Astrometric Standards (CD-ROM distribution). US Naval Obs., Washington
Murray C. A., Penston M. J., Binney J. J., Houk N., 1997, in Battrick B., ed., ESA, *Hipparcos* Venice'97 Symp. ESA Publications, Noordwijk, p. 485
Nilakshi, Sagar, R., Pandey A. K., Mohan V., 2002, A&A, 383, 153
Palla F., Stahler S. W., 1993, ApJ, 418, 414
Pandey A. K., Nilakshi, Ogura, K., Sagar Ram, Tarusawa K., 2001, A&A, 374, 504
Parenago P. P., 1940, AZh, 17, 3
Phelps R. L., Janes K. A., 1993, AJ, 106, 1870
Piatti A. E., Clariá J. J., 2001, A&A, 370, 931
Piatti A. E., Bica E., Santos J. F. C. Jr, Clariá J. J., 2002, A&A, 387, 108
Piskunov A. E., Belikov A. N., 1996, Astron. Lett., 22, 466
Sagar R., Cannon R. D., 1995, A&AS, 111, 75

Sagar R., Cannon R. D., 1997, A&AS, 122, 9
Sagar R., Griffiths W. K., 1991, MNRAS, 250, 683
Sagar R., Griffiths W. K., 1998, MNRAS, 299, 777
Sagar R., Richtler T., 1991, A&A, 250, 324
Sagar R., Munari U., de Boer K. S., 2001, MNRAS, 327, 23
Sanner J., Bruzenderf J., Will J.-M., Geffert M., 2001, A&A, 369, 511
Scalo J., 1986, Fundam. Cosmic Phys., 11, 1
Schaller G., Schaerer D., Meynet G., Maeder A., 1992, A&AS, 96, 269
Schmidt M., 1963, ApJ, 137, 758
Schmidt-Kaler Th., 1982, in Schaifer K., Voigt H. H., eds, Landolt-Berstein Numerical Data and Functional Relationships in Science and Technology, New Series, Group VI, Vol. 2. Springer-Verlag, Berlin, p. 15
Silverman B. W., 1986, Density Estimation for Statistics and Data Analysis. Chapman & Hall, London
Subramaniam A., Sagar R., 1999, AJ, 117, 937
Tout C. A., Pols O. R., Eggleton P. P., Han Z., 1996, MNRAS, 281, 257
Vereschagin S. V., Piskunov A. E., 1992, in Massevich A. G., ed., Chemical evolution of stars and the Milky Way galaxy. Kosmoinform Publications, Moscow, p. 5
Zacharias N. et al., 2000, AJ, 120, 2131

This paper has been typeset from a TEX/LATEX file prepared by the author.